

Outage Performance of Fluid Antenna System (FAS)-aided Terahertz Communication Networks

Leila Tlebaldiyeva, [°]Sultangali Arzykulov, [#]Khaled M. Rabie, [‡]Xingwang Li, and Galymzhan Nauryzbayev
School of Engineering and Digital Sciences, Nazarbayev University, Astana, Z05H0K3, Kazakhstan
[°]CEMSE Division, King Abdullah University of Science and Technology, Thuwal, KSA 23955-6900
[#]Department of Engineering, Manchester Metropolitan University, Manchester, M15 6BH, UK
[‡]School of Physics and Electronic Information Engineering, Henan Polytechnic University, Jiaozuo 454000, China
Emails: {ltlebaldiyeva, galymzhan.nauryzbayev}@nu.edu.kz, [°]sultangali.arzykulov@kaust.edu.sa,
[#]k.rabie@mmu.ac.uk, [‡]lixingwang@hpu.edu.cn

Abstract—Millimeter-wave networks have already been successfully rolled out in many countries and now the research direction heads toward new technologies and standards to enable Tbps rates for future sixth-generation (6G) wireless communication systems. This work studies a point-to-point terahertz (THz) communication network exploiting the concept of a fluid antenna system (FAS) over correlated alpha-mu fading channels, nicely fitting the THz communication. Furthermore, the considered system is expanded to the selection-combining-FAS (SC-FAS) and maximum-gain-combining-FAS (MGC-FAS) diversity variates at the receiver side. The proposed FAS and its diversity configuration techniques are aimed to combat the high path loss, blockages, and molecular absorption effect related to the THz band. Our contribution includes comprehensive outage probability (OP) performance analysis for the THz band given the non-diversity and diversity FAS receivers. Moreover, the derived outage probability formulas are verified via Monte Carlo simulations. Numerical results have confirmed the superior performance of the MGC-FAS scheme in terms of OP. Finally, this work justifies that a higher number of antenna ports dramatically improves the system performance, even in the presence of correlation.

Index Terms— α - μ distribution, correlation, fluid antenna system (FAS), terahertz communication, outage probability.

I. INTRODUCTION

The research toward future communication systems and networks reasonably anticipates the movement of an operating frequency range from the millimeter wave (mmWave) to the terahertz (THz) band that ranges 0.1 – 10 THz to meet the requirement of exponentially growing data demand. This transition provides endless possibilities for ultra-low latency, high-resolution sensing capabilities, and Tbps rates. THz communication enables remarkable applications such as connected robots, autonomous systems, extended reality, digital twins, and holographic teleportation [1]. However, THz communication requires new network architectures and device configurations to make all the remarkable features real. The authors in [2] analyzed the novel and potential antenna types for the THz band and characterized them as low-damage, wide-band, narrow-beam, and with high spectral resolution. The main challenge of novel THz antennas is the non-maturity of manufacturing materials and technology.

The authors in [3] suggested that a software-controlled fluid antenna may replace multiple-input multiple-output (MIMO) antennas for the future generation networks and unleash remarkable properties of fluid antennas such as mechanical flexibility, theoretically infinite diversity, reduced electromagnetic radiation exposure, and exceptional immunity against multi-user interference. The fluid antenna materials, fabrication, and potential applications were discussed in [4]. The authors suggested that non-conventional methods, that are utilized to build Fluid-antenna-systems (FAS) like 3D printing, injecting, or spraying the conductive fluid material on substrates, increase the potential for reconfigurability. The authors in [5] presented a stretchable liquid-metal reconfigurable monopole antenna operating at 2.4 GHz that was designed on the CST program. The authors controlled the resonant frequency by stretching the antenna size and documented 1.8 GHz bandwidth reconfigurability.

The FAS-enabled receivers were studied in [6], [7] for a point-to-point network over correlated Rayleigh fading channels; the outage probability (OP) formulas for FAS-Rx was presented and the FAS performance was compared to the traditional maximum-ratio-combining diversity. The authors in [8] applied a similar system model for an analog beamformed mmWave network and derived the OP formula in a single integral form. The authors in [6]–[9] reported a high performance of the FAS receivers even at a half wavelength size of an antenna length. It is expected that the FAS receivers can obtain more advantages for THz devices. Since the wavelength at THz is in the range of 0.03 – 3 mm, it enables the installation of hundreds of antenna elements on a mobile device, whereas mmWave handheld devices could accommodate up to 32 antenna elements.

Channel modeling is one of the fundamental studies of 6G. The authors in [10] presented a novel framework for modeling realistic THz channels with limited channel-sounding measurements. The proposed paradigm in [10] consists of six phases such as limited channel sounding, calibration of ray tracing simulator, ray tracing simulations, stochastic channel model based on ray, cluster-based channel modeling. The channel measurements at 140 GHz and 220 GHz were conducted for

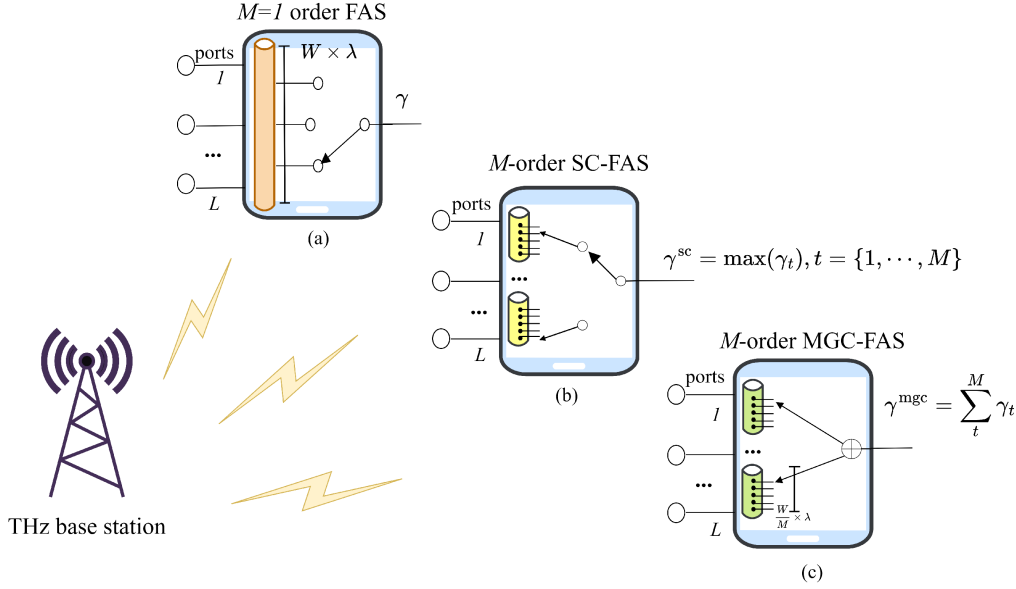


Fig. 1. Schematic of a FAS-aided THz network with the SC-FAS and MGC-FAS diversity configurations.

indoor scenarios in [11], where the authors proposed a single-band close-in path loss model. Moreover, the authors in [12] presented joint multi-path combining clustering and ray-tracing methods to study a signal propagation of THz waves in the indoor scenario and developed a hybrid channel model that applied both ray tracing and statistical methods to model the THz indoor channel. Similarly, the works in [15]–[20] studied indoor THz channel modelling. The authors in [21] investigated popular fading channels with line-of-sight (LOS) components as Rician, Nakagami- m , and $\alpha - \mu$ distributions and compared them with empirical measurements at 142 GHz frequency at different environments (i.e., airport, university, and shopping mall). It was proven that the $\alpha - \mu$ distribution well models the empirical data in the considered environments.

In this work, we study a single-antenna transmitter (Tx) and FAS-enabled receiver with the correlation existing between antenna ports over THz channels. The contributions of this paper are outlined as follows:

- The outage probability is evaluated for the FAS-enabled receivers at practical THz channels by considering a 3D propagation model and the molecular absorption loss.
- The cumulative distribution function (CDF) for the equally correlated $\alpha - \mu$ fading channels for the selection combiner output is presented in this work. To the best knowledge of authors, no prior work studied it before.
- The diversity techniques for FAS-enabled receivers are introduced and their OP performance are investigated.

II. SYSTEM MODEL

A. A Non-diversity FAS Receiver

Assume a THz base station (BS) with a single directional transmit (Tx) antenna communicating to a single FAS receiver (Rx) with L number of antenna ports. FAS-Rx is a tube filled

with a liquid metal of the $W \times \lambda$ size, where $W > 0$ is an antenna size coefficient and λ is a wavelength of the operating frequency. Due to the mobility of the Rx device, there is a Doppler shift effect that causes a correlation between antenna ports. According to [9], the correlation coefficient is evaluated by a closed-form expression over all the ports as

$$r = \frac{2}{L(L-1)} \sum_{k=1}^{L-1} (L-k) J_0 \left(\frac{2\pi k W}{L-1} \right), \quad (1)$$

where J_0 is the zero-order Bessel function of the first kind. Hypothetically, we assume that FAS-Rx contains L ports, mimicing antennas. A voltage controller enables switching to one of the ports, with the highest signal magnitude. For analytical tractability, we do not account for the switching delay of a fluid material.

We consider an independent and identically distributed (i.i.d.) $\alpha - \mu$ channel magnitude $|H_k|$ at k port of FAS-Rx. The maximum selected channel is denoted as $|H_{\max}| = \max_{1 < k < L} \{|H_k|\}$. The CDF of an $\alpha - \mu$ fading channel with envelop $|H_k|$, an arbitrary parameter $\alpha > 0$, which is related to the non-linearity of the propagation medium, and α root mean value $\beta = (E(|H_k|^\alpha))^{\frac{1}{\alpha}}$ is given in [25] as

$$F_{H_k}(x) = \frac{\Gamma(\mu, \frac{x^\alpha \mu}{\beta^\alpha})}{\Gamma(\mu)}, \quad (2)$$

where $\mu > 0$ is the inverse of normalized variance of H_k , $\mu = \frac{E^2(|H_k|^\alpha)}{\text{Var}(|H_k|^\alpha)}$, with $E(\cdot)$ and $\text{Var}(\cdot)$ denoting the expectation and variance operators, and $\Gamma(x) = \int_0^\infty t^{x-1} e^{-t} dt$. The correlated

$\alpha - \mu$ channel amplitude is modelled as

$$H_k = \left(\sum_{j=1}^{\mu} |h_{kj}|^2 \right)^{\frac{1}{\alpha}}, \quad (3)$$

where $|h_{kj}|^2$ is parameterized below

$$h_{kj} = (\sqrt{1-r}X_{kj} + \sqrt{r}Y_{0j}) + i(\sqrt{1-r}Y_{kj} + \sqrt{r}Y_{0j}), \quad (4)$$

where $k = \{1, \dots, L\}$ and $j = \{1, \dots, \mu\}$. X_{0j} , X_{kj} , Y_{0j} , and Y_{kj} are the Gaussian random variables (RVs), with zero mean and 1/2 variance. Furthermore, let us fix $U = \sqrt{r}(X_{0j} + iY_{0j})$ and re-write (4) as

$$h_{kj} = (X_{kj} + iY_{kj})\sqrt{1-r} + U = \tilde{X}_{kj} + i\tilde{Y}_{kj}, \quad (5)$$

where $\tilde{X}_{kj} = X_{kj}\sqrt{1-r} + \sqrt{r}X_{0j}$, $\tilde{X}_{kj} \sim N(\sqrt{r}Y_{0j}, \frac{1-r}{2})$, $\tilde{Y}_{kj} = Y_{kj}\sqrt{1-r} + \sqrt{r}Y_{0j}$, $\tilde{Y}_{kj} \sim N(\sqrt{r}Y_{0j}, \frac{1-r}{2})$, and $h_{kj} \sim C(0, \frac{1}{2})$, $j = 1, \dots, \mu$. Since the channel amplitude is the summation of squared magnitudes of Gaussian RVs, then, H_k^α is the non-central chi-square distribution represented by $H_k^\alpha \sim \chi_{2\mu}^2\left(\sqrt{r}\sum_{j=1}^{\mu}(x_{0j}^2 + y_{0j}^2), \frac{1-r}{2}\right)$, $j = \{1, \dots, \mu\}$ and $X_{0j} = x_{0j}$, $Y_{0j} = y_{0j}$. The CDF of $\chi_n(a, b)$ is given in [22, (2.1.124)], where a^2 is non-centrality parameter and n is the degree of freedom.

B. Propagation Model

In this work, we have adopted a 3D signal propagation model by [23] that accounts for the molecular absorption loss. According to the authors in [24], THz frequencies suffer from the detrimental effect of molecular absorption loss that deteriorates the received signal but also boosts the noise.

The received signal power is formulated as

$$P = \frac{P_t G_1 G_2 c^2}{16\pi^2 f^2 (d^2 + (h_b - h_u)^2 \exp(K(f)(d^2 + (h_b - h_u))))}, \quad (6)$$

where P_t is the transmit power, G_1 is the BS's antenna gain, G_2 is the FAS-Rx gain, c is the speed of light, f is the operating frequency, d is the distance between the BS and user equipment (UE), h_b is the BS height, h_u is the UE's height, $K(f)$ is the molecular absorption loss factor of the transmission medium depending on the operating frequency.

III. OUTAGE PROBABILITY

In this section, we evaluate the outage probability for the FAS-enabled THz networks. For this reason, we should quantify the CDF of the maximum signal-to-noise ratio (SNR) selection in equally correlated $\alpha - \mu$ distribution as

$$\gamma^{\text{fas}} = \max(\gamma_1, \gamma_2, \dots, \gamma_L). \quad (7)$$

The instantaneous SNR γ_k is evaluated as

$$\gamma_k = \frac{PH_k}{N_0}, \quad k = 1, 2, \dots, L, \quad (8)$$

where N_0 is the additive white Gaussian noise (AWGN) per port.

The CDF of equally correlated $\alpha - \mu$ variates is generalized by making use of (3) as

$$\begin{aligned} F_{H_k|U}(x|u) &= \Pr(H_k \leq x|u) \\ &= \Pr\left(\left(\sum_{j=1}^{\mu} |h_{kj}|^2\right)^{\frac{1}{\alpha}} < x\right) \\ &= \Pr\left(\sum_{j=1}^{\mu} |h_{kj}|^2 < x^\alpha\right) \\ &= 1 - Q_\mu\left(\sqrt{\frac{2ru}{1-r}}, \sqrt{\frac{2x^\alpha}{(1-r)\bar{\beta}}}\right), \end{aligned} \quad (9)$$

where $Q_\mu(\cdot, \cdot)$ is the Marcum-Q function and $\bar{\beta} = \frac{\beta^\alpha}{\mu}$. Now, we evaluate the CDF for the FAS output conditioned to the fixed port $U \sim \chi_{2\mu}^2(0, \frac{1}{2})$, $U = \sum_{j=1}^{\mu}(X_{0j}^2 + Y_{0j}^2)$. The conditional CDF is represented as

$$\begin{aligned} F_{\gamma_{\text{sc}}|U}(x|u) &= \Pr(\gamma_1 \leq x^\alpha, \dots, \gamma_L \leq x^\alpha|u) \\ &= \Pr\left(\sum_{j=1}^{\mu} |h_{1j}|^2 \leq \frac{x^\alpha}{\bar{\gamma}}, \dots, \sum_{j=1}^{\mu} |h_{Lj}|^2 \leq \frac{x^\alpha}{\bar{\gamma}}|u\right) \\ &= \left(1 - Q_\mu\left(\sqrt{\frac{2ru}{1-r}}, \sqrt{\frac{2x^\alpha}{(1-r)\bar{\beta}\bar{\gamma}}}\right)\right)^L, \end{aligned} \quad (10)$$

where $\bar{\gamma} = \frac{PE(H_k)}{N_0} = \frac{P}{N_0}$ is the average SNR. Now, by using the probability density function (PDF) of U which is the central chi-square distribution with 2μ degrees of freedom, $U \sim \chi_{2\mu}^2(0, \frac{1}{2})$. By averaging the conditional CDF in (10) over the distribution of $f_U(u) = \frac{u^{\mu-1} e^{-\frac{u}{2}}}{\Gamma(\mu)}$, we get the CDF of the FAS receiver for equally correlated $\alpha - \mu$ distribution as

$$\begin{aligned} F_{\text{sc}}(x) &= \int_0^\infty F_{\text{fas}|U}(x|u) f_U(u) du \\ &= \int_0^\infty \left(1 - Q_\mu\left(\sqrt{\frac{2ru}{1-r}}, \sqrt{\frac{2x^\alpha}{(1-r)\bar{\beta}\bar{\gamma}}}\right)\right)^L \\ &\quad \times \frac{u^{\mu-1} e^{-\frac{u}{2}}}{(2\sigma^2)^\mu \Gamma(\mu)} du. \end{aligned} \quad (11)$$

Finally, the outage probability for FAS-enabled Rx is obtained by using (11) $OP(x) = F_{\text{sc}}(x)$.

A. Diversity FAS Receivers

In this section, we propose the M -order SC-FAS and MGC-FAS diversity techniques and evaluate their outage probability formulas. Fig. 1 illustrates the top view of the non-diversity FAS (a), SC-FAS (b), and MGC-FAS (c). The traditional MGC-combiner technique consider a weighted summation of SNR-branches. In the proposed MGC-FAS technique, we assume that SNR branches are added without being divided into the

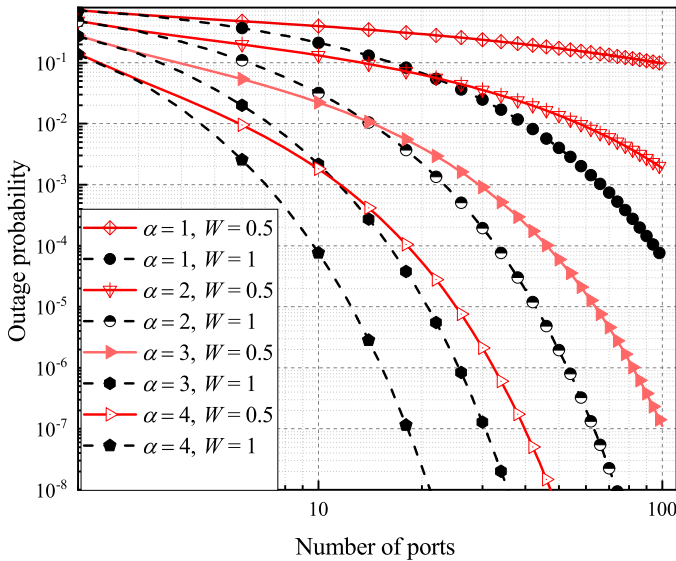


Fig. 2. Outage probability versus the number of ports for the FAS-aided THz network for $\alpha = \{1, 2, 3, 4\}$ and $W = \{0.5, 1\}$ Rx-FAS.

diversity order. The FAS outputs deterministic signal and MGC-FAS sums the SNR from diversity branches. We assume that a FAS tube with $W \times \lambda$ size is divided into M sub-FAS branches with size $\frac{W \times \lambda}{M}$. M -order SC-FAS and MGC-FAS device contain $\frac{L}{M}$ antenna ports per FAS branch. The outage probability for the Rx-enabled SC-FAS is defined by using (11) and by adjusting the antenna ports to $\frac{L}{M}$ as

$$OP^{\text{sc}}(x) = (F_{\text{sc}}(x))^M = \left(\int_0^{\infty} \left(1 - Q_{\mu} \left(\sqrt{\frac{2ru}{1-r}}, \sqrt{\frac{2x^{\alpha}}{\gamma(1-r)}} \right) \right)^{\frac{L}{M}} \frac{u^{\mu-1} e^{-\frac{u}{2\sigma^2}}}{(2\sigma^2)^{\mu} \Gamma(\mu)} du \right)^M. \quad (12)$$

Similarly to the traditional maximum-ratio combining technique, the proposed FAS-MGC diversity technique sums the output SNRs from every FAS tubes as $\gamma_{\text{fas}}^{\text{mgc}} = \sum_{t=1}^M \gamma_t^{\text{fas}}$. The evaluation of the outage probability for the correlated MGC-FAS receivers is mathematically intractable, therefore, we have obtained the outage probability performance by doing Matlab simulations.

$$OP^{\text{mgc}}(x) = \Pr(\gamma_1^{\text{fas}} + \gamma_2^{\text{fas}} \cdots + \gamma_M^{\text{fas}} \leq x^{\alpha}), \quad (13)$$

where γ_t^{fas} is defined in (7).

IV. NUMERICAL SIMULATION

This section presents simulation results obtained from analysis of the outage probability for the FAS-enabled receivers at the THz frequency range. We simulate the THz channel with correlated FAS ports given the following system parameters: Tx power $P_t = 20$ dBm, Tx antenna gain $G_1 = 17$ dBi, Rx antenna gain $G_2 = 14$ dBi, Tx height $h_1 = 4$ m, Rx height

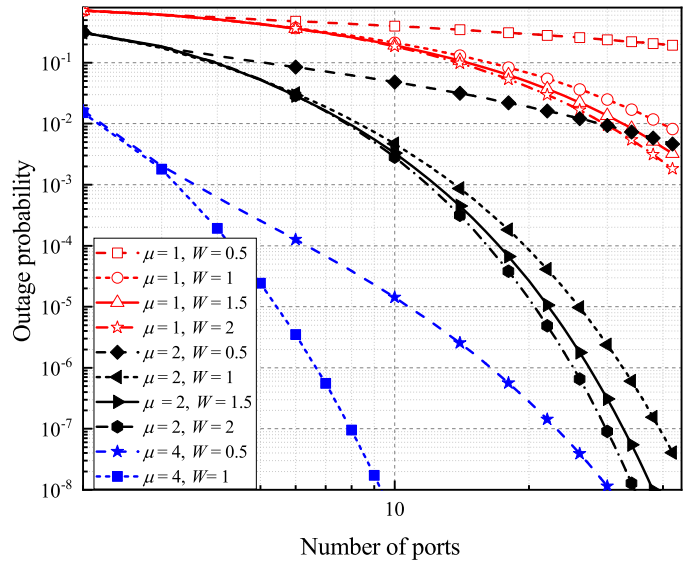


Fig. 3. Outage probability versus the number of ports for the FAS-aided THz network for $\mu = \{1, 2, 4\}$ and $W = \{0.5, 1, 1.5, 2\}$ Rx-FAS.

$h_2 = 1$ m, distance between Tx-Rx is $d = 10$ m, operating frequency $f = 1$ THz, bandwidth is $B = 10$ GHz, $R = 7$ Gbits/s, $K(f) = 0.192 \text{ m}^{-1}$ as in [23], and the range of FAS ports are $L = \{2, 100\}$.

In Fig. 2, we analyze how varying $\alpha = \{1, 2, 3, 4\}$ power parameter and antenna size coefficient $W = \{0.5, 1\}$ affect the outage probability at $\mu = 1$. Let us consider plots for $L = 50$ antenna ports at $W = 1$ and record the following results $OP(\alpha = 1) = 0.237$, $OP(\alpha = 2) = 0.035$, $OP(\alpha = 3) = 9.085 \times 10^{-4}$, $OP(\alpha = 4) = 2.115 \times 10^{-6}$. A higher α value results in a stronger outage probability performance. In addition, we notice that the outage probability performance stays almost the same when $L < 4$ for $W = 0.5$ and $W = 1$ cases. However, when the number of ports increases, there is a noticeable outage probability difference due to the increasing correlation coefficient between ports.

In Fig. 3, we study how channels parameter $\mu = \{1, 2, 4\}$, which identifies the number of multipath clusters, along with the antenna size coefficients $W = \{0.5, 1, 1.5, 2\}$ at the fixed $\alpha = 1$ affect the outage probability performance. Given the same antenna size coefficient, $W = 0.5$ and different μ -parameter values produce a substantial difference in the OP performance. For instance, for $L = 10$ ports, the outage probability of $OP(\mu = 1) = 0.42$, $OP(\mu = 2) = 0.047$, $OP(\mu = 4) = 1.5 \times 10^{-5}$ are recorded at $\mu = \{1, 2, 4\}$. It means that a higher number of multipath clusters significantly increases the outage probability. At the same time, the smallest antenna size coefficient $W = 0.5$ results in a lower outage probability performance in comparison to other counterparts due to a higher effect of correlation between ports. For instance, at $L = 20$ and $\mu = 2$ outage probability is recorded as $OP(W = 0.5) = 0.0187$, $OP(W = 1) = 8.574 \times 10^{-5}$, $OP(W = 1.5) = 2.653 \times 10^{-5}$, $OP(W = 2) = 1,357 \times$

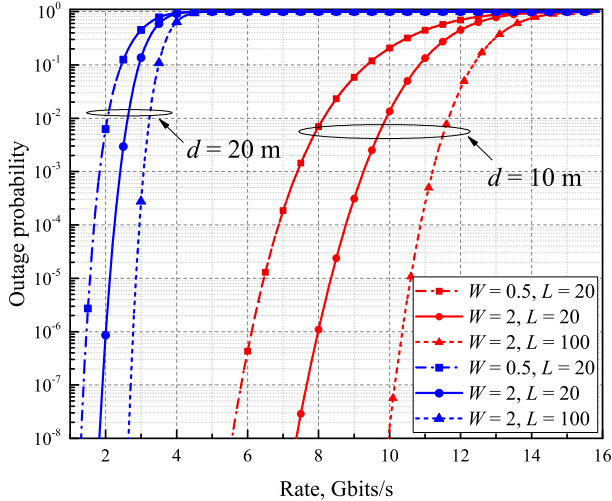


Fig. 4. Outage probability versus rate for the FAS-aided THz network for $\mu = 2$, $W = \{0.5, 2\}$, and $d = 10, 20$ m Rx-FAS.

10^{-5} . Hence, there is 218 times performance improvement from $W = 0.5$ plot to $W = 1$ case. Moreover, this figure demonstrates that an increasing number of antenna ports dramatically enhances the outage probability for all scenarios. Specifically let us consider plots for $\mu = 2$ and $W = 0.5$ the OP is obtained as $OP(L = 10) = 0.048$, $OP(L = 20) = 0.018$, $OP(L = 30) = 0.009$, $OP(L = 40) = 0.005$, $OP(L = 50) = 0.003$, $OP(L = 60) = 0.002$, and $OP(L = 100) = 3.703 \times 10^{-4}$. So, from $L = 10$ to $L = 100$ case there is a 130 times outage probability performance enhancement.

In Fig. 4, we analyze how the distance between the base station and receiver, antenna size, and the number of antenna ports reflect on the outage probability. For this reason, we consider the following environment $\alpha = 2$, $\mu = 2$, and the Rx-FAS with $L = \{20, 100\}$ and $W = \{0.5, 2\}$. If we consider $L = 20$ and $d = 10$ m scenario for the $W = \{0.5, 2\}$ FAS, then we observe around 2 Gbits/s rate difference from a $W = 0.5$ to $W = 2$ case. Similarly, we observe 6 Gbits/s rate improvement from $L = 20$ to $L = 100$ antenna ports per receiver FAS. In other words, a higher number of antenna ports has a higher impact on the network performance. Similar observations are made for the $d = 20$ m plots. Furthermore, the distance is a crucial factor in the THz range, even 10 m difference creates 4 times decrease in achievable rate to meet $OP = 10^{-4}$ at $W = 2$ and $L = 20$ scenario. For instance, at $L = 20$ m and $W = 2$ to obtain performance of $OP = 10^{-4}$, we obtain following rates at 10m and 20m distances as $R(10m) = 8.8$ Gbits/s and $R(20m) = 2.37$ Gbits/s. Furthermore, this figure demonstrates that one could combat a high path loss at the THz range by using FAS with a higher number of ports.

In Fig. 5, we compare the $M = \{2, 4\}$ -order MGC-FAS and SC-FAS with the non-diversity FAS receiver for

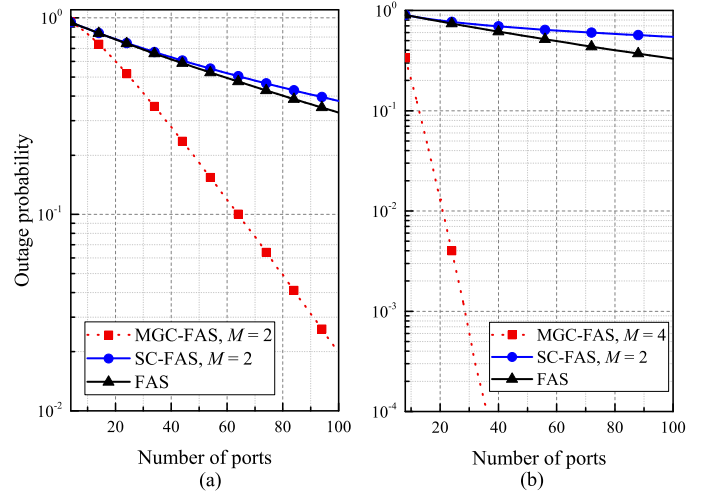


Fig. 5. Outage probability versus the number of ports for the non-diversity FAS, MGC-FAS, and SC-FAS.

$L = 100$ ports. It means that for $M = 2$ -order FAS there are two FAS tubes with $L = 50$ ports each. For simulation purposes we use $W = 2$, $\mu = 2$, $\alpha = 2$, $R = 9$ Gbits/s, and $d = 13$ m. For clarity purposes, we consider two sub-plots for $M = 2$ (a) and $M = 4$ diversity orders of SC-FAS and MGC-FAS. There are several important observations made from this figure. The MGC-FAS diversity scheme demonstrates the highest performance among all plots. As the number of diversity branches increases in the MGC-FAS the performance also significantly improves. For instance, $M = 4$ -order MGC-FAS with $L = 8$ results in $OP(M = 4) = 0.3368$, whereas, $M = 2$ -order MGC-FAS returned $OP^{mgc}(M = 2) = 0.8745$. Oppositely, the SC-FAS scheme demonstrates a lower performance when the number of diversity orders rises from $M = 2$ to $M = 4$. For example, $OP^{sc}(M = 2, L = 32) = 0.68$ and $OP^{sc}(M = 4, L = 32) = 0.072667$. Next, the L -port FAS slightly outperforms the $M = 2$ -order SC-FAS scheme.

V. CONCLUSION

One of the candidate technologies for 6G is the THz communication ranging in (0.1 – 10 THz) spectrum. In this work, we aimed to model a THz channel by considering 3D propagation model of the signal and molecular absorption effect of THz band. We suggested using the FAS-enabled receivers to improve the end-user performance. The proposed model is analytically tractable and provides important insights in the analysis of THz networks. We analyzed both non-diversity and diversity FAS receivers in terms of the outage probability formulas. Simulation results demonstrated that a non-diversity FAS outperforms the SC-FAS, however, it demonstrates a significantly lower performance rather than the MGC-FAS scheme. Moreover, simulation results reveal that the higher values of α and μ channel parameters, more antennas and antenna ports improve the system performance.

REFERENCES

- [1] C. Chaccour, M. N. Soorki, W. Saad, M. Bennis, P. Popovski and M. Debbah, "Seven Defining Features of Terahertz (THz) Wireless Systems: A Fellowship of Communication and Sensing," *IEEE Communications Surveys & Tutorials*, vol. 24, no. 2, pp. 967-993, Secondquarter 2022.
- [2] Y. He, Y. Chen, L. Zhang, S. W. Wong and Z. N. Chen, "An overview of terahertz antennas," *China Communications*, vol. 17, no. 7, pp. 124-165, July 2020.
- [3] K.K. Wong, K.F. Tong, Y. Zhang, and Z. Zhongbin, "Fluid Antenna System for 6G: When Bruce Lee Inspires Wireless Communications," *Electronics Letters*, vol. 56, no. 24, pp. 1288-1290, Nov. 2020.
- [4] K. N. Paracha, A. D. Butt, A. S. Alghamdi, S. A. Babale, and P. J. Soh, "Liquid Metal Antennas: Materials, Fabrication and Applications," *Sensors*, vol. 20, no. 1, p. 177, Dec. 2019.
- [5] D. Hensley, C. Christodoulou and N. Jackson, "A Stretchable Liquid Metal Reconfigurable Monopole Antenna," *2020 IEEE International Symposium on Antennas and Propagation and North American Radio Science Meeting*, 2020, pp. 585-586.
- [6] K. -K. Wong, A. Shojaeifard, K. -F. Tong and Y. Zhang, "Fluid Antenna Systems," *IEEE Transactions on Wireless Communications*, vol. 20, no. 3, pp. 1950-1962, Mar. 2021.
- [7] K. K. Wong, A. Shojaeifard, K. -F. Tong and Y. Zhang, "Performance Limits of Fluid Antenna Systems," *IEEE Communication Letters*, vol. 24, no. 11, pp. 2469-2472, Nov. 2020.
- [8] L. Tlebaldiyeva, G. Nauryzbayev, S. Arzykulov, A. Eltawil and T. Tsiftsis, "Enhancing QoS Through Fluid Antenna Systems over Correlated Nakagami- m Fading Channels," *2022 IEEE Wireless Communications and Networking Conference (WCNC)*, 2022, pp. 78-83.
- [9] K. K. Wong, K. F. Tong, Y. Chen, and Y. Zhang, "Closed-form expressions for spatial correlation parameters for performance analysis of fluid antenna systems," *Electronics Letters*, Apr. 2022.
- [10] K. Guan, H. Yi, D. He, B. Ai and Z. Zhong, "Towards 6G: Paradigm of realistic terahertz channel modeling," *China Communications*, vol. 18, no. 5, pp. 1-18, May 2021.
- [11] J. He, Y. Chen, Y. Wang, Z. Yu and C. Han, "Channel Measurement and Path-Loss Characterization for Low-Terahertz Indoor Scenarios," *2021 IEEE International Conference on Communications Workshops (ICC Workshops)*, 2021, pp. 1-6.
- [12] Y. Chen, Y. Li, C. Han, Z. Yu and G. Wang, "Channel Measurement and Ray-Tracing-Statistical Hybrid Modeling for Low-Terahertz Indoor Communications," *IEEE Transactions on Wireless Communications*, vol. 20, no. 12, pp. 8163-8176, Dec. 2021.
- [13] C.X. Wang, J. Huang, H. Wang, X. Gao, X. You and Y. Hao, "6G Wireless Channel Measurements and Models: Trends and Challenges," *IEEE Vehicular Technology Magazine*, vol. 15, no. 4, pp. 22-32, Dec. 2020.
- [14] S. Priebe, C. Jastrow, M. Jacob, T. Kleine-Ostmann, T. Schrader, and T. Kurner, "Channel and propagation measurements at 300 GHz," *IEEE Transactions on Antennas and Propagations*, vol. 59, no. 5, pp. 1688-1698, May 2011.
- [15] S. Kim, W. T. Khan, A. Zaji 'c, and J. Papapolymerou, "D-band channel measurements and characterization for indoor applications," *IEEE Transactions on Antennas and Propagations*, vol. 63, no. 7, pp. 3198-3207, Jul. 2015.
- [16] S. Kim and A. Zaji 'c, "Characterization of 300-GHz wireless channel on a computer motherboard," *IEEE Transactions on Antennas and Propagations*, vol. 64, no. 12, pp. 5411-5423, Dec. 2016.
- [17] C.L. Cheng, S. Kim, and A. Zaji 'c, "Comparison of path loss models for indoor 30 GHz, 140 GHz, and 300 GHz channels," *Proc. 11th European Conference on Antennas Propagation (EuCAP)*, Mar. 2017, pp. 716-720.
- [18] S. L. H. Nguyen, J. Järveläinen, A. Karttunen, K. Haneda, and J. Putkonen, "Comparing radio propagation channels between 28 and 140 GHz bands in a shopping mall," *Proc. 12th European Conference on Antennas Propagation (EuCAP)*, 2018, pp. 1-5.
- [19] J. M. Eckhardt, T. Doeker, S. Rey, and T. Kürner, "Measurements in a real data centre at 300 GHz and recent results," *Proc. 13th European Conference on Antennas Propagation (EuCAP)*, Mar. 2019, pp. 1-5.
- [20] Y. Xing, O. Kanhere, S. Ju, and T. S. Rappaport, "Indoor wireless channel properties at millimeter wave and sub-terahertz frequencies," *Proc. IEEE Global Communication Conference (GLOBECOM)*, Dec. 2019, pp. 1-6.
- [21] E. N. Papatotiriou, A.-A. A. Boulogeorgos, K. Haneda, M. F. de Guzman, and A. Alexiou, "An experimentally validated fading model for THz wireless systems," *Scientific Reports*, vol. 11, no. 1, Sep. 2021.
- [22] J. G. Proakis, "Digital Communications," 3rd ed. New York: McGrawHill, 1995.
- [23] A. Shafie, N. Yang, Z. Sun and S. Durrani, "Coverage Analysis for 3D Terahertz Communication Systems with Blockage and Directional Antennas," *2020 IEEE International Conference on Communications Workshops (ICC Workshops)*, 2020, pp. 1-7.
- [24] C. Chaccour, M. N. Soorki, W. Saad, M. Bennis, P. Popovski and M. Debbah, "Seven Defining Features of Terahertz (THz) Wireless Systems: A Fellowship of Communication and Sensing," *IEEE Communications Surveys & Tutorials*, vol. 24, no. 2, pp. 967-993, Secondquarter 2022.
- [25] M. D. Yacoub, "The α - μ Distribution: A Physical Fading Model for the Stacy Distribution," *IEEE Transactions on Vehicular Technology*, vol. 56, no. 1, pp. 27-34, Jan. 2007.
- [26] K. Yoshikawa and T. Hayashi, "Experimental Study of Loss and Variation of Human Blockage for Terahertz Wireless Communications," *2022 16th European Conference on Antennas and Propagation (EuCAP)*, 2022, pp. 1-5.